CHIN. PHYS. LETT. Vol. 38, No. 4 (2021) 045201

Generation of a Plasma Waveguide with Slow-Wave Structure

Xiao-Bo Zhang(张小波), Xin Qiao(乔鑫), Ai-Xia Zhang(张爱霞), and Ju-Kui Xue(薛具奎)*

College of Physics and Electronics Engineering, Northwest Normal University, Lanzhou 730070, China

(Received 5 November 2020; accepted 1 February 2021; published online 6 April 2021)

Using the particle-in-cell simulations, we report an efficient scheme to generate a slow wave structure in the electron density of a plasma waveguide, based on the array laser–plasma interaction. The spatial distribution of the electron density of the plasma waveguide is modulated via effective control of the super-Gaussian index and array pattern code of the lasers. A complete overview of the holding time, and the bearable laser's intensity of the electron density structure of the plasma waveguide, is obtained. In addition, the holding time of the slow wave structure of the plasma waveguide is also controlled by adjusting the frequency of the array laser beam. Finally, effects due to ion motion are discussed in detail.

DOI: 10.1088/0256-307X/38/4/045201

Extending laser-plasma interaction length using an extended plasma waveguide has many potential applications, such as laser-driven electron accelerators,[1–3] soft x-ray lasers,[4,5] and high-harmonic generation.[6] A variety of technologies have been proposed to further improve the quality of these photon and particle sources, to modulate the density profile of plasma waveguide, which facilitates an improvement in the transverse energy of the electron, and to fulfill phase-matching conditions.[7,8] Corrugated "slow-wave" plasma structures are generated by ionizing the cluster source in a cryogenically supersonic gas jet, which supports the guided propagation of a high-intensity laser, and can realize different waveguide lengths for different cluster gases.[9] Moreover, a plasma waveguide with a slow-wave structure has demonstrated positive effects in terms of the quasi phase-matched direct laser acceleration of charged particles, and the generation of a wide spectrum of electromagnetic radiation.[9–11] Furthermore, by periodically obstructing the cluster flow with an array of thin wires, a cluster-based plasma waveguide can be modulated axially.[12,13] However, the application of the waveguide for different schemes necessitates the replacement of diffractive optics or wire obstructions in the gas jet, which raises difficulties in terms of its optimization in specific applications.

One novel development to enhance laser–plasma interaction is primarily based on the design for structured interfaces, i.e., a laser-driven micro plasma waveguide.[14–20] Ordered nanowire arrays, irradiated by femto-second laser pulses, can volumetrically heat dense matter into a new ultrahot plasma.[15] The enhancement of the x-ray production is realized by the modification of local electric fields near the surface nanostructures.[18,19] A micro-channel plasma target is used to enhance and manipulate laser-driven electron sources in the solid density regime.[14,16,17] A novel mechanism to produce high yield positrons is also proposed, whereby a microstructured surface target (MST) is irradiated by a femto-second laser.[20,21] Although novel microstructures, and waveguides with a slow wave structure, can greatly improve the performance of the interaction between laser and plasma, and facilitates the manipulation of the interaction, the combination of micro-channel plasma targets and slow-wave structures is still worth exploring, since it could effectively extend applications involving laser–plasma interaction. Moreover, due to the formation of underdense plasma caused by the ionization of solid material in the cavity of the microstructure target, the modulation of these ionized electrons is also critical for the secondary exploitation and structural design of the microstructure target.

In this Letter, a slow wave structure in the electron density of the plasma waveguide is effectively realized via the array's laser–plasma interaction. The array's laser pulses can be generated by an argon fluoride laser source and a tiled fiber laser array,[22,23] and underdense plasma can be produced via single-photon ionization of a lithium-vapor column.[24,25] A ponderomotive force in the laser, including both transverse and longitudinal components, is generated inside the plasma, and modulates the spatial distribution of the electrons to obtain a slow-wave structure in the electron density. The characteristic parameters of the plasma waveguide are effectively controlled by the adjustment of the super-Gaussian index, and the array

Supported by the National Natural Science Foundation of China (Grant Nos. 11865014, 11765017, 11764039, 11475027, 11274255, and 11305132), the Natural Science Foundation of Gansu Province (Grant No. 17JR5RA076), and the Scientific Research Project of Gansu Higher Education (Grant No. 2016A-005).

*Corresponding author. Email: xuejk@nwnu.edu.cn

© 2021 Chinese Physical Society and IOP Publishing Ltd

pattern code of the lasers. The holding-time scale of the plasma waveguide is discussed in detail; this can also be increased by correctly adjusting the frequency of the array laser beam. The bearable laser's intensity in terms of the electron density structure, and the effects of ions, are also discussed in some depth.

Simulation Setup. We consider the interaction of an array laser and underdense plasma to generate a slow-wave structure in the electron density of the plasma waveguide, via particle-in-cell (PIC) simulations. Our two-dimensional (2D) PIC simulations are performed using VSim software,[26] which solves the coupled Vlasov–Maxwell equations. The laser pulse is y-polarized, and propagates along the z direction. The electric field of the laser beam, as experienced by the underdense plasma, can be given by $\boldsymbol{E} = E_{0\mathrm{L}}\alpha(y)\beta(t)e^{-i(\omega t-kz)}\hat{\boldsymbol{y}}$, where $E_{0\mathrm{L}}$ is the laser field amplitude, $\omega_0 = 1\times10^{16}\,\mathrm{rad{\cdot}s^{-1}}$ is the laser frequency; $\alpha(y) = \sum_{n=-m}^{n=m}\exp[-(\frac{y+nd}{b_\mathrm{w}})^q]$ is used to specify the beam profile, $b_\mathrm{w} = 1\,\mu\mathrm{m}$ is the beam width, $d = 2b_\mathrm{w}$ is the array separation distance, and q is a variable known as the super-Gaussian (SG) index; $\beta(t) = \sin(\pi t/\tau_0)^2$ and $\tau_0 = 1\,\mathrm{fs}$ denote the pulse width. The plasma frequency is $\omega_\mathrm{pe} = 1.1\times10^{12}\,\mathrm{rad\cdot s^{-1}}$, and the initial density is $N_0 = 4\times10^{20}\,\mathrm{m^{-3}}$. The initial plasma is uniform in both transverse and longitudinal directions. The length and width of the plasma are $3\,\mu\mathrm{m}$, and $12\,\mu\mathrm{m}$, respectively. The ion in the plasma is $\mathrm{H^+}$. Moreover, the initial temperature of the electron and ion is zero, because the plasma is cold. The interaction of the laser and plasma takes place in a simulation box of $4\times14\,\mu\mathrm{m}^2$ (400×1400 cells) in the $z\times y$ dimensions. Each cell contains 2×2 macro-particles, representing the ensemble of real charged particles, and the time step is $\Delta t = 8.7\,\mathrm{as}$. An absorbing boundary is used in the PIC simulations. In the discussion of the PIC simulation results, the relevant physical parameters are written in the dimensionless form, using the scalings: $t\sim t/\omega_0^{-1}$, $\omega\sim\omega/\omega_0$, $\omega_\mathrm{pe}\sim\omega_\mathrm{pe}/\omega_0$, $\boldsymbol{r}\sim\boldsymbol{r}/c\omega_0^{-1}$, and $N\sim N/N_0$, $\boldsymbol{p}\sim\boldsymbol{p}/mc$, and $E\sim Ee/m\omega_0 c$, N_0 is the initial density of the plasma.

Generation and Holding Time of the Slow-Wave Structure. Simulation results for the normalized electron density near the axis ($y/b_\mathrm{w}\approx0$, first row) and edge ($y/b_\mathrm{w}\approx1$, second row) of the plasma waveguide versus time are shown in Figs. 1(a1)–1(a4). For the case generated by the Gaussian laser ($q=2$) with array pattern code $m=0$ (the first column), in the initial process ($t<0.45\times10^3$), the transverse ponderomotive force of the laser gradually pushes the electrons located at the axis of the laser to the edge of the laser. Meanwhile, the longitudinal ponderomotive force of the laser pushes the electrons to the propagation direction of the laser [Figs. 1(a1) and 1(a3)]. In other words, the electron density of the plasma exhibits weak non-uniform characteristics, i.e., a slow-wave structure with weak amplitude [Fig. 1(b1)]. Over the time period $0.45\times10^3 < t < 1.35\times10^3$, an electrostatic field is generated, and increases gradually, which results from the charge separation of the electrons and ions. When the longitudinal component of the ponderomotive force gradually approaches the longitudinal component of the electrostatic field force, the electrons are no longer pushed by longitudinal ponderomotive force, and the structure of the electrostatic field will be unchanged. Given that the laser propagates along the z direction, the structure of the electrostatic field is generated periodically, corresponding to the obvious formation of a high-density region near the edge of the laser, and a low-density region near the axis of the laser [Figs. 1(b3) and 1(b5)]. It is interesting to note that the electrons located at the high and low density region are effectively modulated by the short pulse, and exhibit periodical distribution in the longitudinal direction [Figs. 1(a1) and 1(a3)], indicating the successful realization of a slow-wave structure in the plasma waveguide. Finally, owing to the fact that the transverse ponderomotive force is greater than the transverse component of the electrostatic field force, the electrons located at the axis of the laser are continuously pushed to the edge of the laser, breaking the slow-wave structure [Figs. 1(a1) and 1(a3)] and generating the plasma channel [Fig. 1(b7)]. The signal plasma channel is generated gradually over time [Fig. 1(c1)]. Clearly, the employment of the short pulse leads to the appearance of a slow wave structure in the plasma waveguide over a certain time period. Since the ponderomotive force of the laser depends on the pulse width and the transverse distribution of the laser, the period length of the slow-wave structure is controlled by the pulse width of the laser.[27] When the array pattern code equals 1 (see the second column in Fig. 1), there is an effective modulation of the plasma waveguide in the transverse direction. In the initial process, the electron space distribution [Figs. 1(a2), 1(a4), and 1(b2)] is similar to the case of $m=0$ [Figs. 1(a1), 1(a3), and 1(b1)]. Specifically, the electron density is modulated to generate a multi-plasma waveguide with a slow-wave structure in the time period $0.45\times10^3 < t < 1.35\times10^3$ [Figs. 1(a2), 1(a4), 1(b4), and 1(b6)]. In addition, due to the effects of the array laser, there are three plasma channels with a periodic high density boundary when the irradiation time of the laser is greater than 1.35×10^3 [Figs. 1(b8) and 1(c2)]. In other words, the modulation for the electron distribution patterns, based on the interaction of the array laser and the plasma, not only realizes the slow wave structure in the longitudinal direction, but also paves the way for the design for structured interfaces of plasma wave guides in the transverse direction.

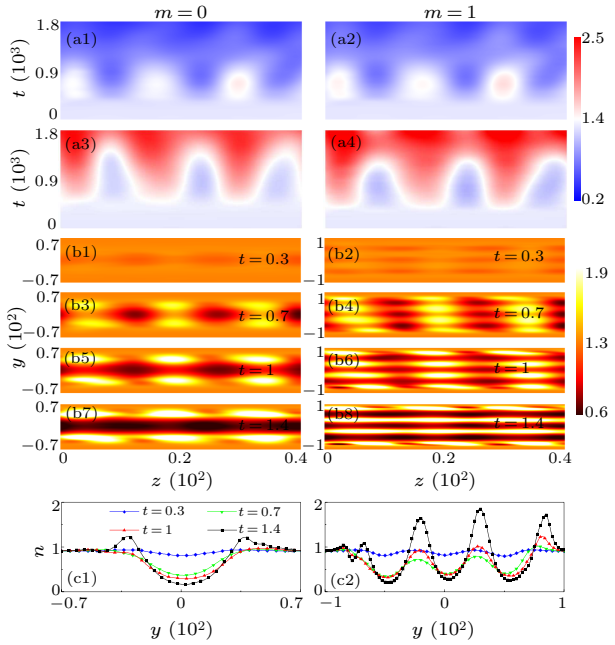

Fig. 1. Variation in electron density near the axis (a1), (a2) and the edge (a3), (a4) of the laser versus time t. The corresponding variation in electron density across the z and y axes for different time $t(\times 10^3)$ (b1)–(b8). The transverse distribution of the electron density for different times, where the longitudinal location is 0.27×10^2 (c1) and (c2). The first (second) column for the array pattern code $m = 0$ ($m = 1$). Here $\omega = 1$, $E_{0L} = 0.03$, $q = 2$.

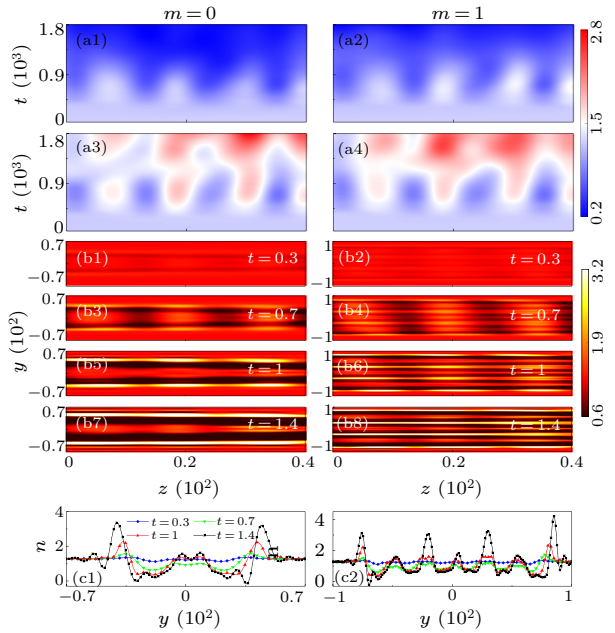

Fig. 2. The same as Fig. 1 but for the super-Gaussian index $q = 6$.

Figure 2 shows the results generated by a super-Gaussian laser ($q = 6$) with an array pattern-code for the array laser beam of $m = 0$ (the first column) and $m = 1$ (the second column). Clearly, the electron density is basically uniform when $0 < t < 0.45 \times 10^3$ [Figs. 2(b1) and 2(b2)]. The periodic density distribution of the high and low density region is also formed gradually when the time increases from 0.45×10^3 to 1.1×10^3 [Figs. 2(b3), 2(b4), 2(b5), and 2(b6)]. The periodic density distribution of the low density region disappears gradually when $t > 1.1 \times 10^3$ [Figs. 2(a1), 2(a2), 2(b7), and 2(b8)]. Meanwhile, a plasma channel is also generated effectively [Figs. 2(c1) and 2(c2)]. Note that when the plasma is irradiated by the super-Gaussian array laser, there is an obvious decrease in the width, and a concomitant increase in the number of the plasma waveguide, as compared with that generated by the Gaussian laser ($q = 2$, see Fig. 1), which results from the fact that the higher SG index has a steeper and larger field gradient, generating a larger amount of ponderomotive force. The longitudinal distribution of the high density shows a significant nonlinear structure when the time is greater than 1.1×10^3, which not only reduces the holding time of the slow-wave structure, but also makes the realization of the slow wave structure more difficult [Figs. 2(a3) and 2(a4)]. In other words, the width and the number of a plasma waveguide with slow-wave structure can be simultaneously modulated by changing the SG index of the array laser.

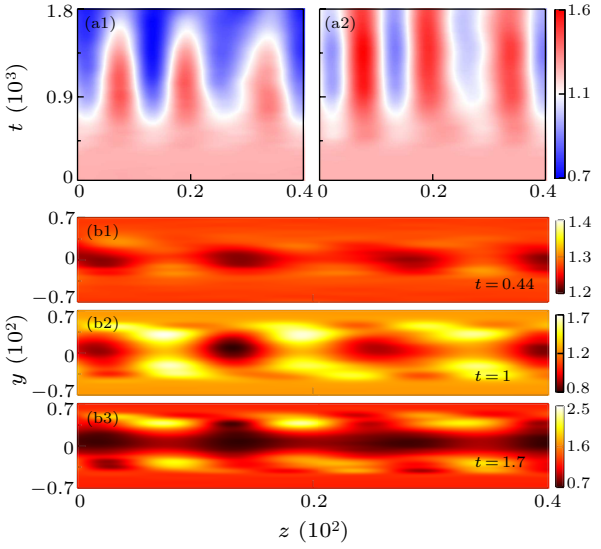

Fig. 3. Variation of the electron density near the axis (a1) and the edge (a2) of the laser versus time t, with a Gaussian laser ($q = 2$). The spatial distributions of the electron density at the transverse y–z plane for different times $t(\times 10^3)$ (b1)–(b3). Here $\omega = 2$, $E_{0L} = 0.03$.

Although the periodic density distribution of the electrons can hold for 1×10^3 (i.e., 0.1 ps), to generate a slow-wave structure with $m = 0$ and micro-scale electron structures with $m = 1$, the holding time of the electrons' structure can also be controlled by adjusting the frequency of the laser. Figures 3(a1) and 3(a2) show the variation in the electron density of the low density region and high density region, respectively, generated by a Gaussian laser ($q = 2$) versus time t, when the frequency of the laser is $\omega = 2$. When $0 < t < 0.45 \times 10^3$, the electron density of

the low-density and high-density regions exhibit weak non-uniform characteristics in the longitudinal direction. The corresponding density distribution of the electrons against y and z is shown in Fig. 3(b1). When $0.45 \times 10^3 < t < 1.2 \times 10^3$, the spatial structure of the electrons is significantly affected by the periodic density distribution, resulting in the formation of a slow-wave structure in the plasma [Figs. 3(a1), 3(a2), and 3(b2)]. Moreover, the effects of the periodic density distribution in the low-density region gradually weaken when $t > 1.35 \times 10^3$ [Figs. 3(a1) and 3(b3)]. However, the high-density region maintains a periodic density distribution in the $0.45 \times 10^3 < t < 1.8 \times 10^3$ range [Figs. 3(a2) and 3(b3)]. In the case of the super-Gaussian laser ($q = 6$), modulation of the frequency of the laser can also effectively increase the holding time of the periodic density distribution of the electrons.

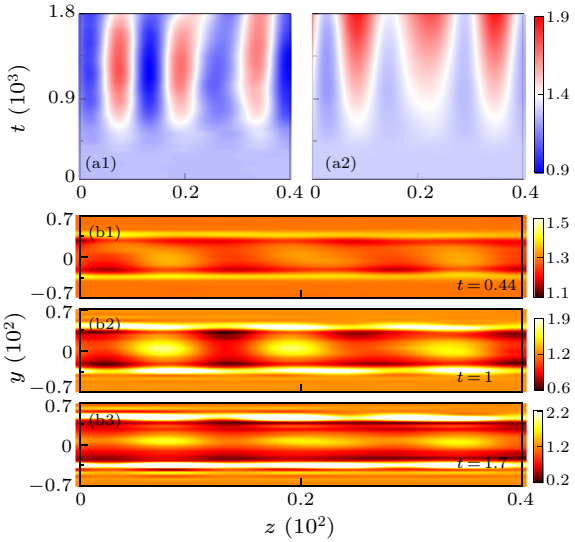

Fig. 4. The same as Fig. 3 but for a super-Gaussian index $q = 6$.

Figures 4(a1) and 4(a2) show the variation in the electron density of the low-density region and the high-density region, respectively, generated by the super-Gaussian laser ($q = 6$), versus time t, where the frequency of the laser is $\omega = 2$. When the time is less than 0.45×10^3, the electron density exhibits weak non-uniform characteristics in the longitudinal direction. The corresponding density distribution of the electrons against y and z [Fig. 4(b1)] is similar to the results of the Gaussian laser shown in [Fig. 3(b1)]. When $t > 0.45 \times 10^3$, the low-density region is modulated by the short pulse to generate the periodic density distribution of the electrons [Figs. 4(a1), 4(a2), and 4(b2)]. As the time increases, the effects of the periodic density distribution gradually strengthen for the high-density region [Figs. 4(a1) and 4(b3)]. However, the high density region maintains its periodic density distribution [Figs. 4(a2) and 4(b3)]. In other words, the holding time of the periodic density distribution generated by the Gaussian and the super-Gaussian laser can be increased from 1×10^3 to 1.4×10^3 (i.e., 0.1 ps to 0.14 ps) when the frequency of the laser is $\omega = 2$.

Effects of Laser Intensity and Ion Motion. Next, we discuss in detail the effects of laser intensity with respect to the realization of controllable electron density patterns. Figure 5 illustrates the variations in electron density near the regime of $y = 0$ as a function of laser intensity and longitudinal location, based on the array pattern-codes $m = 0$ (the first column) and $m = 1$ (the second column). When the intensity of the Gaussian laser beam increases from 0.03 to 0.22, the periodical distribution of the electron density near the $y = 0$ region disappears gradually. Once the laser's intensity exceeds 0.22, the periodic distribution of the electron density is completely replaced by uniform distribution of the electron density [Figs. 5(a) and 5(b)]. For the super-Gaussian laser beam, periodic distribution of the electron density is realized only when the laser's intensity is located within the $0.03 < E_{0L} < 0.16$ range. In addition, when the laser intensity is greater than 0.16, the periodic distribution of the electron density is completely broken [Figs. 5(c) and 5(d)].

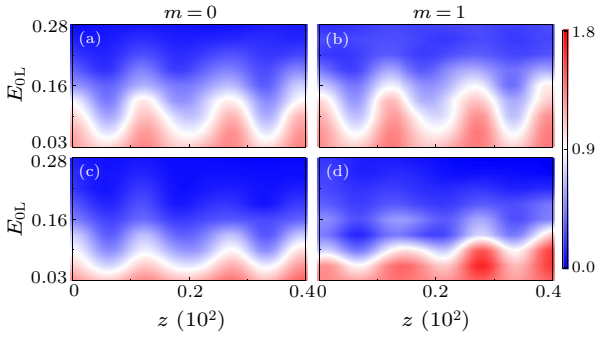

Fig. 5. The variation in electron density near the axis of the laser ($y = 0$) versus laser intensity E_{0L}, and the longitudinal coordinate z with a Gaussian laser (the first row) and a super-Gaussian laser (the second row). In the first (second) column for the array pattern code, $m = 0$ ($m = 1$). Here $\omega = 1$, $t = 0.7 \times 10^3$.

Moreover, the amplitude of the periodical distribution of the electron density generated by the array laser beam when $m = 1$ is clearly stronger than that generated by the laser beam when $m = 0$. The equations of motion of the electron in the light field is $\partial_\eta(\gamma u_\perp - a) = 0$ and $\partial_\eta(\gamma u_z - \gamma) = 0$, where $\eta = z - t$, γ is the relativistic factor, u is the velocity of the electrons, and a is the normalized vector potential of the laser. Given that the initial velocity of the electron is zero, the equations of motion of the electron can be expressed by $\gamma u_\perp = a$ and $\gamma u_z = \gamma - 1 = a^2/2$.[28,29] Clearly, for the nonrelativistic laser ($a < 1$), the transverse velocity of the electron is greater than the longitudinal velocity of the electron. When the intensity

of the laser is near to or greater than the intensity of the relativistic laser ($a \to 1$ and $a > 1$), the longitudinal velocity of the electron will be near to and greater than the transverse velocity of the electron, resulting in the electrons of the plasma being pushed along the propagation direction of the laser; this will not generate a slow-wave structure. To clarify the physical mechanism of the effects of laser intensity on the realization of a controllable plasma waveguide, the effect of the laser's intensity on the average momentum, $(\bar{p}_y, \bar{p}_z)$, of the electrons, and the difference in the transverse momentum, $\bar{p}_y$, and the longitudinal momentum, $\bar{p}_z$, are shown in Fig. 6. For the Gaussian laser beam and super-Gaussian laser beam, the $\bar{p}_y$ value is much greater than the $\bar{p}_z$ value when the laser's intensity is less than 0.23. As the laser's intensity increases from 0.23 to 1.2, $\bar{p}_z$ is close to $\bar{p}_y$, and the difference between the $\bar{p}_y$ and $\bar{p}_z$ is gradually reduces to zero. Although the intensity of $\bar{p}_y$ and $\bar{p}_z$ improves significantly, the difference between $\bar{p}_z$ and $\bar{p}_z$ is not significantly affected when the array pattern-code $m = 1$. Clearly, the $\bar{p}_y$ generated by the transverse ponderomotive force $F_{p\perp}$ is the key factor in the formation of a controllable plasma waveguide with a slow-wave structure. Once $\bar{p}_z$ is close to $\bar{p}_y$, the electrons are pushed to the front of the plasma, rather than to the edge of the laser, which breaks the plasma waveguide.

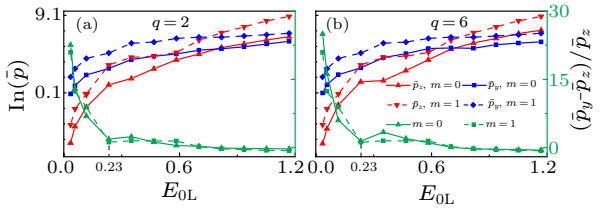

Fig. 6. Average momentum $(\bar{p}_y, \bar{p}_z)$ of the electrons, and the momentum difference between the $\bar{p}_y$ and $\bar{p}_z$. $[(\bar{p}_y - \bar{p}_z)/\bar{p}_z$, green line] against the intensity of the Gaussian laser (a) and super-Gaussian laser (b) at $t = 0.7 \times 10^3$.

Figure 7 shows the average velocity $(\bar{v}_e, \bar{v}_i)$ of electrons and ions relative to time for different types of laser beam. As the time increases from 0 to 2.6×10^3, $\bar{v}_e(\bar{v}_i)$ is accelerated to $0.5 \times 10^{-2}c$ $(0.2 \times 10^{-5}c)$. When the array pattern-code is set to $m = 1$, the electrons and ions achieve a higher velocity, where $v_e(\approx 1.15 \times 10^{-2}c)$, and $v_i(\approx 0.57 \times 10^{-2}c)$ [Fig. 7(a)]. For the super Gaussian laser beam, where $m = 1$, the average velocity of the electrons and ions shows a slight increase in the same variation trend [Fig. 7(b)]. Clearly, in the generation process of different plasma waveguides, $\bar{v}_i$ is far less than the $\bar{v}_e$, which implies that the moving ions do not affect the lifetime of the ideal electron density structure.

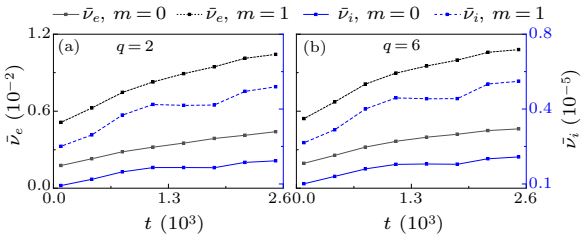

Fig. 7. Variation of the average velocity of electrons (black line) and ions (blue line) versus time t, with Gaussian laser (a) and super-Gaussian laser (b). $E_{0L} = 0.03$.

In conclusion, we have achieved an efficient scheme, based on laser-plasma interaction in a uniform and cold plasma, to generate a controllable slow-wave structure in the electron density of a plasma waveguide. The width and number of the plasma waveguide is effectively modulated and controlled by a super-Gaussian index, together with the array pattern-code of the array laser beam. Meanwhile, the longitudinal slow-wave structure can also be adjusted via the width of the laser pulse. In particular, we have focused on holding time and sustainable laser intensity in relation to micro-scale structures in the plasma. We have provided a detailed explanation for the effects of ion movement with respect to the generation of a plasma waveguide. Such powerful and simple modulation techniques in relation to electron density represent a novel approach to realizing a slow-wave structure of electron density in plasma waveguides.

References

[1] Geddes C G R, Toth C, van Tilborg J, Esarey E, Schroeder C B, Bruhwiler D, Nieter C, Cary J and Leemans W P 2004 *Nature* **431** 538
[2] Leemans W P, Nagler B, Gonsalves A J, Toth C, Nakamura K, Geddes C G R, Esarey E, Schroeder C B and Hooker S M 2006 *Nat. Phys.* **2** 696
[3] Ho Y C, Hung T S, Yen C P, Chen S Y, Chu H H, Lin J Y, Wang J and Chou M C 2011 *Phys. Plasmas* **18** 063102
[4] Kneip S, McGuffey C, Martins J L, Martins S F, Bellei C, kov V C, Dollar F, Fonseca R, Huntington C, Kalintchenko G, chuk A M, Mangles S P D, Matsuoka T, Nagel S R, Palmer C A J, Schreiber J, Phuoc K T, Thomas A G R, Yanovsky V, Silva L O, Krushelnick K and Najmudin Z 2010 *Nat. Phys.* **6** 980
[5] Cipiccia S, Islam M R, Ersfeld B, Shanks R P, Brunetti E, Vieux G, Yang X, Issac R C, Wiggins S M, Welsh G H, Anania M P, euski D M, Montgomery R, Smith G, Hoek M, Hamilton D J, Lemos N R C, Symes D, Rajeev P P, Shea V O, Dias J M and Jaros-zynski D A 2011 *Nat. Phys.* **7** 867
[6] Kuo C C, Pai C H, Lin M W, Lee K H, Lin J Y, Wang J and Chen S Y 2007 *Phys. Rev. Lett.* **98** 033901
[7] Hung T S, Ho Y C, Chang Y L, Wong S J, Chu H H, Lin J Y, Wang J and Chen S Y 2012 *Phys. Plasmas* **19** 063109
[8] Chien T Y, Chang C L, Lee C H, Lin J Y, Wang J and Chen S Y 2005 *Phys. Rev. Lett.* **94** 115003
[9] Layer B D, York A, Antonsen T M, Varma S, Chen Y H, Leng Y and Milchberg H M 2007 *Phys. Rev. Lett.* **99** 035001
[10] Corde S, Phuoc K T, Lambert G, Fitour R, Malka V, Rousse A, Beck A and Lefebvre E 2013 *Rev. Mod. Phys.*

85 1
[11] York A G, Milchberg H M, Palastro J P and Antonsen T M 2008 *Phys. Rev. Lett.* **100** 195001
[12] Yoon S J, Goers A J, Hine G A, Magill J D, Elle J A, Chen Y H and Milchberg H M 2013 *Opt. Express* **21** 15878
[13] Hine G A, Goers A J, Feder L, Elle J A, Yoon S J and Milchberg H M 2016 *Opt. Lett.* **41** 3427
[14] Snyder J, Ji L L, George K M, Willis C, Cochran G E, Daskalova R L, Handler A, Rubin T, Poole P L, Nasir D, Zingale A, Chowdhury E, Shen B F and Schumacher D W 2019 *Phys. Plasmas* **26** 033110
[15] Kaymak V, Pukhov A, Shlyaptsev V N and Rocca J J 2016 *Phys. Rev. Lett.* **117** 035004
[16] Ji L L, Snyder J and Shen B F 2019 *Plasma Phys. Control. Fusion* **61** 065019
[17] Zou D B, Pukhov A, Yi L Q, Zhuo H B, Yu T P, Yin Y and Shao F Q 2017 *Sci. Rep.* **7** 42666
[18] Rajeev P P, Ayyub P, Bagchi S and Kumar G R 2004 *Opt. Lett.* **29** 2662
[19] Mondal S, Chakraborty I, Ahmad S, Carvalho D, Singh P, Lad A D, Narayanan V, Ayyub P, Kumar G R, Zheng J and Sheng Z M 2011 *Phys. Rev. B* **83** 035408
[20] Wang Y C, Yin Y, Wang W Q, Zou D B, Miao W X, Yu T P and Shao F Q 2020 *Sci. Rep.* **10** 5861
[21] Palastro J P, Antonsen T M, Morshed S, York A G and Milchberg H M 2008 *Phys. Rev. E* **77** 036405
[22] Cheung E C, Ho J G, Goodno G D, Rice R R, Rothenberg J, Thielen P, Weber M and Wickham M 2008 *Opt. Lett.* **33** 354
[23] Bakhtiari F, Golmohammady S, Yousefi M and Ghafary B 2016 *Phys. Plasmas* **23** 123105
[24] Wang S, Clayton C E, Blue B E, Dodd E S, Marsh K A, Mori W B, Joshi C, Lee S, Muggli P, Katsouleas T, Decker F J, Hogan M J, Iverson R H, Raimondi P, Walz D, Siemann R and Assmann R 2002 *Phys. Rev. Lett.* **88** 135004
[25] Hogan M J, Assmann R, Decker F J, Iverson R, Raimondi P, Rokni S, Siemann R H, Walz D and Whittum D 2000 *Phys. Plasmas* **7** 2241
[26] *The Particle-In-Cell software by Tx-Corp* https://www.txcorp.com/vsim
[27] Kong Q, Miyazaki S, Kawata S, Miyauchi K and Nakajima K *et al.* 2003 *Phys. Plasmas* **10** 4605
[28] Cruer W L 1988 *The Physics of Laser Plasma Interactions* (Boca Raton: CRC Press)
[29] Teubner U, Bergmann J, Wonterghem B *et al.* 1993 *Phys. Rev. Lett.* **70** 794